Towards Understanding of the Selective Precipitation of Alkali Metal Cations in Presence of Dipicrylamine Anion

Suresh Eringathodi,[a] Pragati Agnihotri,[a] Bishwajit Ganguly,[a] Pragnya Bhatt,[a] Palani Sivagnana Subramanian,[a] Parimal Paul*[a] and Pushpito K. Ghosh*[a]

Keywords: Dipicrylamine / Alkali and alkaline earth metals / Selectivity / Single-crystal X-ray structure / Structure-selectivity correlation

Dipicrylamine anion (DPA^-) precipitates out [K(DPA)] with high selectivity from salt bitterns containing Na^+, K^+, and Mg^{2+}, whereas the same ligand shows poor selectivity towards K^+ – and much higher selectivity towards Cs^+ – in studies conducted with a mixture of K^+, Rb^+, and Cs^+. Their single-crystal structures reveal that the K^+ and Rb^+ salts have similar layered structures, with 8 oxygen atoms from seven DPA^- anions encapsulating the metal cation, whereas the Cs^+ salt possesses a channel-like structure with the metal ion encapsulated by ten oxygen atoms from six DPA^-. The conformation of DPA^- in the [Cs(DPA)] single crystal matches closely that of DPA in crystalline state. M···O and intermolecular C–H···O interactions together stabilize the structures. The ^{133}Cs NMR spectrum of the poorly soluble [Cs(DPA)] shows an upfield shift of the peak with respect to CsCl as a result of the interaction with the oxygen atoms of DPA^-, whereas ^{23}Na NMR spectrum of the highly soluble [Na(DPA)] shows no such upfield shift compared to NaCl. Powder XRD patterns of bulk [M(DPA)] (M = K^+, Rb^+, and Cs^+) precipitates show that these are similar to the patterns obtained by simulation of the single-crystal X-ray data. The selectivity of precipitation correlates qualitatively with the size and hydration enthalpies of the ions.

Introduction

Dipicrylamine (2,2′,4,4′,6,6′-hexanitrodiphenylamine, DPA) anion (Figure 1) has been used for the extraction of K^+ from sea bittern (mixture of K^+, Na^+, and Mg^{2+}).[1] The process of such extraction is depicted in Scheme 1. In a study conducted with a mixture of K^+, Rb^+, and Cs^+, it has been reported that the Cs^+ ion shows maximum selectivity towards DPA.[2] Indeed, recovery of Cs^+ from radioactive waste has been reported.[3] In spite of the large number of reports on the utility of DPA^-, little is known about the factors which control its selectivity towards the different alkali and alkaline earth metal ions.

DPA possesses some interesting structural features, namely: (i) six nitro groups that are flexible and can interact and adjust in the space, (ii) a secondary amine group that can be deprotonated with $Ca(OH)_2$ to form a water soluble salt, and (iii) partial delocalization of the resultant charge mediated by the aromatic rings, that may facilitate coordination of the oxygen atoms with suitable metal ions. Single-crystal X-ray structures of DPA and some of its organic

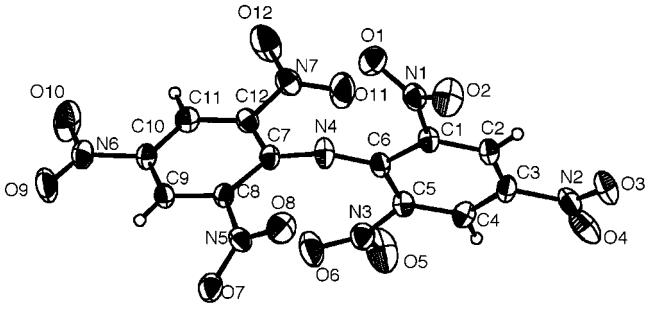

Figure 1. ORTEP view of the deprotonated dipicrylamine (DPA^-) showing atom numbering scheme.

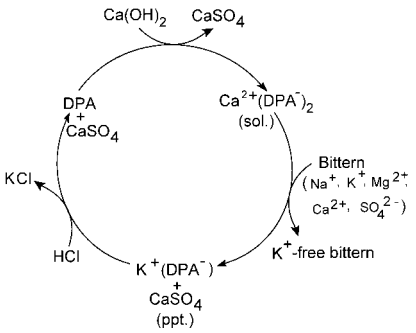

Scheme 1. Cyclic diagram showing extraction of KCl from bittern using DPA and $Ca(OH)_2$ and recycling of DPA.

[a] Analytical Science Discipline, Central Salt and Marine Chemicals Research Institute,
Bhavnagar 364002, India
E-Mail: pkghosh@csmcri.org (P. K. Ghosh)
ppaul@csmcri.org (P. Paul)

Supporting information for this article is available on the WWW under http://www.eurjic.org or from the author.

salts have been reported.[4] Computational study on the intermolecular interactions observed in the crystal structure of DPA has also been reported recently.[5] Crystal structures of K^+ and Ag^+ salts of DPA^- have been reported, although no detailed analysis of the former compound was carried out in absence of adequate refinement of the structure.[6a,6b] In the case of Rb^+ and Cs^+ salts of DPA^-, only unit cell parameters have been reported earlier.[6b–6d]

Herein, we report quantitative ion-chromatographic studies of DPA^- selectivity towards bittern and an equimolar aqueous mixture of K^+, Rb^+, and Cs^+ salts. We also report the synthesis and single-crystal X-ray structures of K^+, Rb^+, and Cs^+ salts of DPA^- to unravel the causes underlining selectivity, and further show that the powder XRD patterns simulated from these structures tally well with those of the bulk precipitated salts. ^{133}Cs and ^{23}Na solution NMR studies of the poorly soluble and highly soluble DPA^- salts of Cs^+ and Na^+, respectively, were also undertaken. These studies have enabled us to understand the possible factors that govern observed selectivity.

Results

Ion Selectivity

Ion selectivity was estimated by analyzing the composition of metal ions in the precipitate formed upon addition of $Ca(DPA)_2$ into aqueous mixtures of cations, as described in the experimental section. Our initial study was focused on the selectivity towards K^+ in bittern. The concentrations of Na^+, K^+, Mg^{2+}, and Ca^{2+} in bittern used for this study were estimated to be 0.8 M, 1.2 M, 2.1 M, and 0.2 M, respectively, from ion chromatographic analysis of the bittern. The precipitate obtained upon addition of $Ca(DPA)_2$ into bittern was similarly analyzed for the metal ion composition after destructive degradation of the complex. The chromatogram shows complete absence of Mg^{2+} despite its high concentration in bittern whereas the relative concentration of K^+ was found to 97.1% (Figure S1, Supporting Information, see also the footnote on the first page of this article). Na^+ and Ca^{2+} were present in the chromatograms to the extent of 2.7% and 0.2%, respectively, but these peaks were found even for a blank chromatogram with Milli Q water. The high selectivity evident for K^+ was reproducible on larger scale and corroborates earlier findings of high selectivity.[1] However, when the studies were conducted with equimolar mixture of KCl, RbCl, and CsCl, the observed selectivities were: 2.6%, 6.6%, and 90.7% for K^+, Rb^+, and Cs^+, respectively, i.e., very poor selectivity towards K^+ in marked contrast to the behavior found with bittern.[1]

Synthesis of the Complexes

[M(DPA)] [M = Na^+ (**1**), K^+ (**2**), Rb^+ (**3**), and Cs^+ (**4**)] salts of alkali metal ions were synthesized. The K^+, Rb^+, and Cs^+ salts **2**–**4** were synthesized by the reaction of the respective metal chloride salts with aqueous solution of the soluble $Ca(DPA)_2$. The K^+ salt has also been prepared following the same method using bittern instead of aqueous solution of metal chloride. The Na^+ salt **1** could not, however, be synthesized by this method because of its very high solubility in water. **1** was instead prepared from the reaction of NaOH and DPA in water followed by evaporation of solvent to dryness. All these compounds gave satisfactory elemental analysis. UV/Vis spectra of **1**–**4** in water were similar; the only band observed for all compounds showing similar λ_{max} (426 nm) and molar absorptivity ($\varepsilon \approx 3.5 \times 10^4$ $M^{-1}cm^{-1}$). X-ray quality single crystals of **2**, **3**, and **4** were grown by slow evaporation of the respective aqueous solutions at room temperature. However, attempts to grow the crystals of **1** were unsuccessful.

Crystal Structures

[K(DPA)]·0.5H_2O (2) and [Rb(DPA)]·H_2O (3): Crystallographic data for complexes **2, 3** and **4** are summarized in Table 4. Compounds **2** and **3** are isostructural. The DPA^- anions in these structures are arranged in a manner that allows the metal ions to interact strongly with eight nitro oxygen atoms of the DPA^- ligands, which is similar to that found in the crystal structure of [K(DPA)], reported earlier.[6a] PLUTO view of **2** showing the metal–oxygen interactions are illustrated in Figure 2. Oxygen atoms (O5 and O6) of one of the *o*-nitro groups (N3) are not involved in interaction with metal ion, otherwise at least one oxygen atom from all other nitro groups makes strong M···O interactions. The interacting metal–oxygen distances for **2** (Table 1) are in the range of 2.767 to 3.022 Å (average K–O distance is 2.916 Å), which is close to the value of 2.76 to 3.04 Å found earlier for [K(DPA)]. In the case of **3**, the Rb–O distances are in the range of 2.911 to 3.150 Å, with average Rb–O distance of 3.023 Å (Table 1). These values are comparable to the reported metal–oxygen distances.[7] In the case of N5 and N7 nitro groups, all of the four oxygen atoms (O7, O8, O11, and O12) interact with the metal ion, in which O7 shows μ-type interaction involving the neighboring metal ion. The K···K and Rb···Rb distances in **2** and **3** are 4.413 and 4.835 Å, respectively. Values of the mean plane distortion between the two phenyl rings of the DPA^- in **2** and **3** are 78.78° and 79.75°, respectively. The two *o*-nitro groups, N1–O1/O2 and N5–O7/O8, are rotated with respect to the phenyl rings to which they are attached by 33.7° and 32.40° in **2** and 34.22° and 31.3° in **3**, respectively.

Figure 3 shows the packing diagram of **2** viewed down the *a* axis. The metal ions and the lattice water molecules are located between the adjacent ligand layers running along the *c* axis in the overall layered architecture. The corrugated organic layer formed in the case of **2** is held in place by C–H···O interaction between the phenyl H11 hydrogen with the O10 nitro oxygen along *c*-direction, and between the phenyl H9 hydrogen and O3 nitro oxygen from the adjacent corrugated organic layer almost along *b* axis. These interactions create the layered architecture. The oxygen

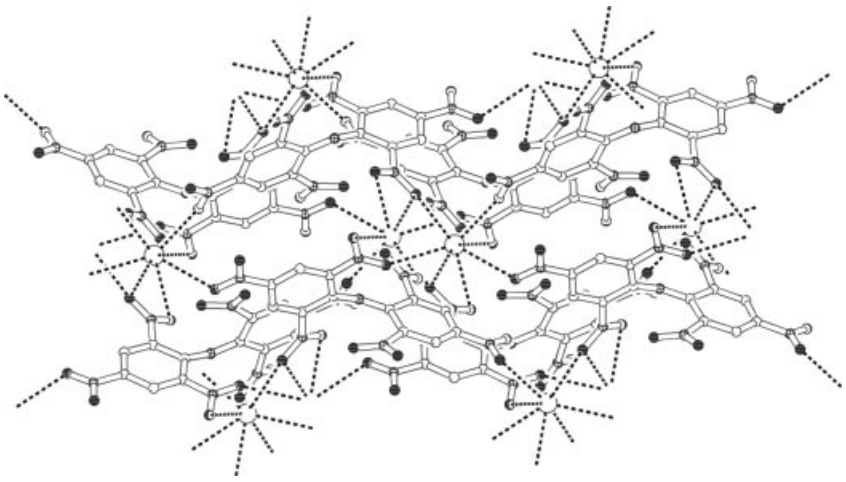

Figure 2. PLUTO view of [K(DPA)] (**2**) showing the interaction between the metal ion (open circle) and oxygen atoms (dark circles) of DPA^-.

Table 1. Metal–oxygen distances [Å] for **2**, **3**, and **4**.

Compound **2**			
K(1)–O(4)[a]	2.767(3)	K(1)–O(2)	2.814 (3)
K(1)–O(7)[b]	2.910(3)	K(1)–O(8)[b]	2.911(3)
K(1)–O(12)[c]	2.922(3)	K(1)–O(7)[d]	2.973(3)
K(1)–O(11)[e]	3.008(4)	K(1)–O(9)	3.022(3)
Compound **3**			
Rb(1)–O(3)	2.911(2)	Rb(1)–O(2)	2.941(2)
Rb(1)–O(11)[f]	3.001(2)	Rb(1)–O(7)	3.024(2)
Rb(1)–O(8)	3.050(2)	Rb(1)–O(9)	3.050(2)
Rb(1)–O(7)[g]	3.057(2)	Rb(1)–O(12)	3.150(3)
Compound **4**			
Cs(1)–O(1)	3.268(3)	Cs(1)–O(3)[l]	3.303(3)
Cs(1)–O(1)[h]	3.268(3)	Cs (1)–O(4)[k]	3.410(2)
Cs(1)–O(3)[i]	3.305(3)	Cs (1)–O(4)[l]	3.410(2)
Cs(1)–O(3)[j]	3.305(3)	Cs (1)–O(5)[m]	3.280(4)
Cs(1)–O(3)[k]	3.303(3)	Cs (1)–O(5)[n]	3.280(4)

[a] $x - 1/2, -y + 3/2, z - 1/2$. [b] $x - 1/2, -y + 1/2, z + 1/2$. [c] $x, y, z + 1$. [d] $-x + 1/2, y + 1/2, -z + 1/2$. [e] $-x, -y + 1, -z$. [f] $-x + 1, -y + 2, -z$. [g] $x + 2, -y + 2, -z$. [h] $-x, y, 1/2 - z$. [i] $1/2 + x, 1/2 + y, z$. [j] $-1/2 - x, 1/2 + y, 1/2 - z$. [k] $-1/2 - x, 1/2 - y, 1 - z$. [l] $1/2 + x, 1/2 - y, -1/2 + z$. [m] $x, 1 + y, z$. [n] $-x, 1 + y, 1/2 - z$.

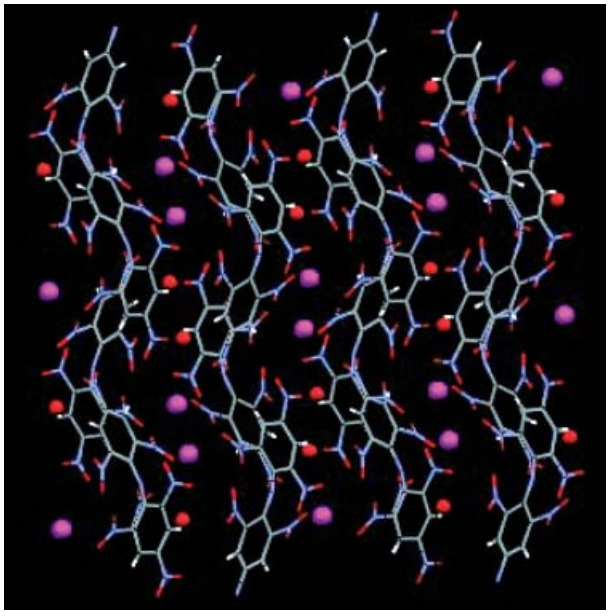

Figure 3. Molecular packing diagram of $[K(DPA)]\cdot 0.5H_2O$ (**2**) showing the architecture, in which the metal ions (purple) are encapsulated in regular intervals. Oxygen atoms of entrapped water molecules are shown in red.

Table 2. Parameters of C–H···O interactions for **2**, **3**, and **4**.

D–H···A [Å]	H···A [Å]	D···A [Å]	< D–H···A [°]
Compound **2**			
C(4)–H(4)···O(1)w[a]	H(4)···O(1)w = 2.44(4)	C(4)···O(1)w = 3.337(10)	C(4)–H(4)···O(1)w = 178 (4)
C(9)–H(9)···O(3)[b]	H(9)···O(3) = 2.58(4)	C(9)···O(3) = 3.417(5)	C(9)–H(9)···O(1)w = 176(4)
C(11)–H(11)···O(10)[c]	H(11)···O(10) = 2.51(4)	C(11)···O(11) = 3.389(6)	C(11)–H(11)···O(10) = 167(4)
Compound **3**			
C(4)–H(4)···O(1)w[d]	H(4)···O(1)w = 2.45(2)	C(4)···O(1)w = 3.337(4)	C(4)–H(4)···O(1)w = 175(2)
C(11)–H(11)···O(10)[e]	H(11)···O(10) = 2.43(3)	C(11)···O(11) = 3.400(3)	C(11)–H(11)···O(10) = 159(3)
Compound **4**			
C(4)–H(4)···O(1)[f]	H(4)···O(1) = 2.42(1)	C(4)···O(1) = 3.278(4)	C(4)–H(4)···O(1) = 154(2)

[a] x, y, z. [b] $1 - x, 1 - y, 1 - z$. [c] $-x, 1 - y, -z$. [d] $1- x, 1 - y, -z$.[e] $1 + x, y, z$. [f] $x, -y, 1/2 + z$.

atom of the lattice water molecule also interacts with the H4 hydrogen of the phenyl ring. These observations are in contrast to the earlier report, where it was stated that no intermolecular interactions were found. The water molecule seen in the lattice of the present structure was also not observed in the earlier structure.[6a] In the case of **3**, only one C–H···O intermolecular interaction along *c* axis exists forming the corrugated layer as mentioned above for **2**, but no cross linking C–H···O interaction connecting the adjacent layers is observed. This could be due to the larger ionic radius of Rb^+ compared to K^+, and also inclusion of more water molecules between the layers, which prevents the sterically hindered ligands from coming closer to make such interaction along the *b* axis. The water molecules in **3** exhibit strong C–H···O interactions with a single DPA^- ligand, whereas in the case of **2** similar interactions of the water molecules with two DPA^- ligands are evident. Details of the H-bonding interactions found in complexes **2**, **3**, and **4** are given in Table 2.

[Cs(DPA)] (4): The molecule crystallises in centrosymmetric space group *C*2/*c* with Cs atom occupying a special position falling in the two-fold axis passing through the amino nitrogen atom of the deprotonated DPA moiety. Ten oxygen atoms of the surrounding nitro groups from six ligands make strong interactions with the metal ion. The PLUTO diagram showing the metal-oxygen interactions is depicted in Figure 4. At least one oxygen atom of each nitro group from the symmetry-related DPA ligand is involved in Cs···O interactions, the distances of which are in the range of 3.268 to 3.410 Å (average distance is 3.313 Å). These are in close agreement with the reported values.[7e,8] Oxygen atoms, O3 and O4, which are attached to N2, interact with the same metal ion; in addition O3 also makes μ-type of interaction involving the neighbouring metal ion. The Cs···Cs distance observed in this structure is 5.788 Å. The mean plane distortion between the phenyl rings of the DPA^- is 61.35°, while the *o*-nitro group N1–O1/O2 is rotated by 23.79° with respect to the phenyl ring to which it is attached.

The molecular packing (Figure 5) and C–H···O interactions in this molecule are quite different from that found in **2** and **3**. The H4 hydrogen atom shows strong intermolecular C–H···O interaction with O1 oxygen atoms of the *o*-nitro groups of a neighbouring molecule of DPA^-. Four such pairs of ligands assemble to create cavities down the *c* axis, in which the Cs^+ is encapsulated making interactions with the surrounding ten oxygen atoms from six ligands. The hydrogen bonding parameters with symmetry code is given in Table 2.

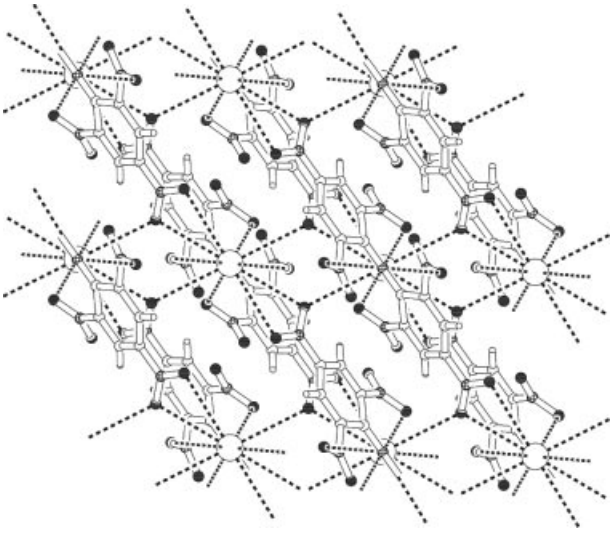

Figure 4. PLUTO view of [Cs(DPA)] (**4**) showing the interaction between the metal ion (open circles) and oxygen atoms (dark circles) of DPA^-.

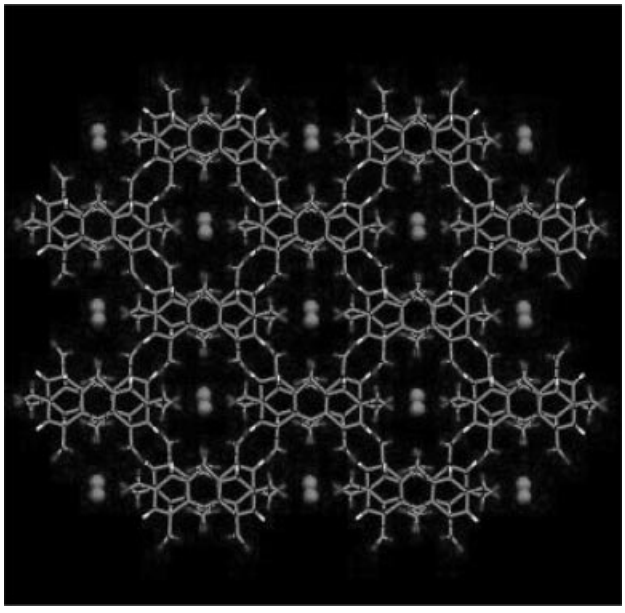

Figure 5. Molecular packing diagram of [Cs(DPA)] (**4**) showing the architecture, in which the metal ions (solid circles) are encapsulated in regular intervals.

NMR Study

To investigate possible differences in the coordination environments of metal ions in **1** and **4**, ^{23}Na and ^{133}Cs NMR spectra of the corresponding compounds were recorded and compared with those of NaCl and CsCl, respectively, in D_2O. ^{23}Na signal of **1** (Figure 6b′) appeared at the same position as of NaCl (Figure 6a′). In the case of **4**, on the other hand, the ^{133}Cs signal (Figure 6b) was shifted upfield significantly compared to that of CsCl (Figure 6a). Initially, soon after preparation of the solution, one signal was observed at –49.70 ppm (considering the signal of CsCl at 0.0 ppm), however, after 20 min, an additional signal appeared at –31.12 ppm (Figure 6c), and finally after 1 h, a third signal of low intensity appeared at –20.19 ppm (Figure 6d).

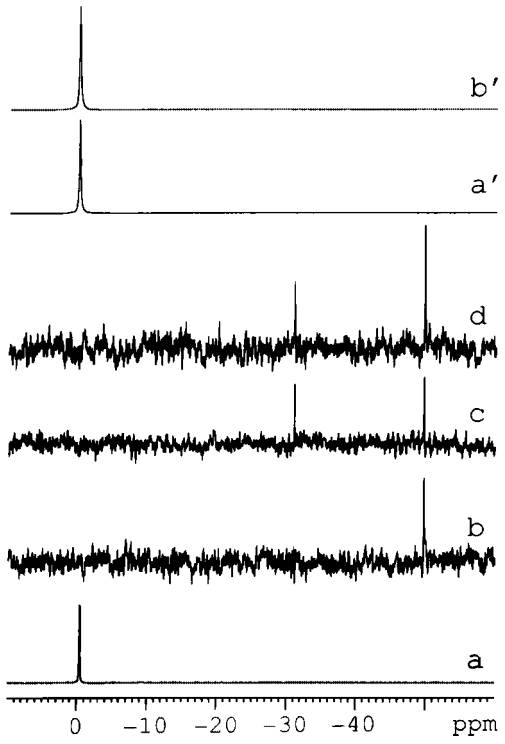

Figure 6. ^{133}Cs NMR spectra of CsCl (a) and [$Cs^+(DPA)^-$], recorded just after making solution (b), after 20 min (c) and after 60 min (d); and ^{23}Na NMR spectra of NaCl (a′) and [$Na^+(DPA)^-$] (b′). All spectra were recorded at room temperature in D_2O. Chemical shift position was taken as 0 ppm for the chloride salts of Na^+ and Cs^+.

Powder X-ray Diffraction

Powder XRD profiles of bulk precipitates of **2**–**4** obtained spontaneously upon addition of a solution of pure salt of the alkali metal ion into aqueous $Ca(DPA)_2$ were recorded. The XRD patterns of the same compounds **2**–**4** were also generated by simulation from the single-crystal X-ray data (Figure 7). The simulation was carried out following the method of Speak.[9] Good match between the experimental and simulated diffractograms was found. The diffractogram was also recorded of the highly water soluble **1** by evaporating the aqueous solution to dryness to obtain a solid powder. Unit cell parameters of **1**–**4** obtained from Powder XRD data and that of **2**–**4** obtained from single-crystal X-ray is shown in Table 3. The unit cell of **1** obtained from powder XRD data was found to be triclinic

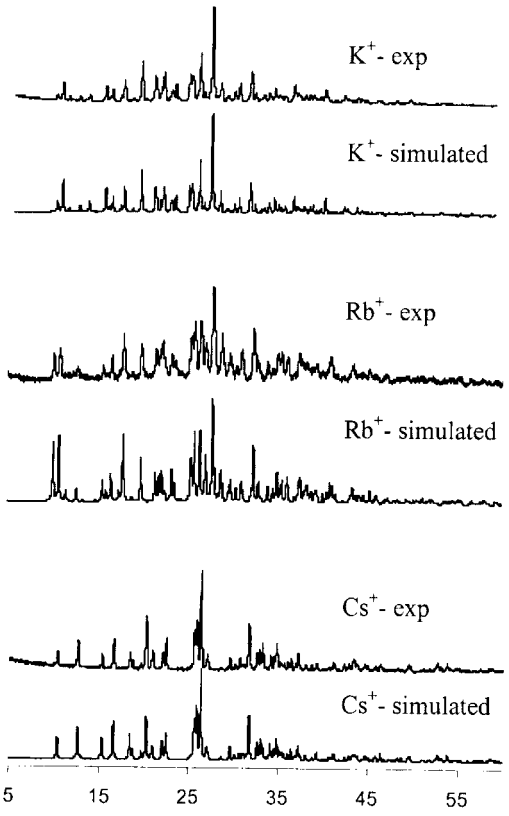

Figure 7. Experimental powder XRD data of bulk precipitates of K^+, Rb^+, and Cs^+ salts of DPA^- vs. powder XRD patterns simulated from the single-crystal X-ray data of the corresponding crystalline salts grown from the bulk precipitates.

Table 3. Crystal systems and unit cell parameters obtained from powder and single-crystal X-ray diffraction data for DPA and its compounds **1**–**4**.

DPA/complexes	Method	Crystal system	Unit cell dimensions *a*, *b*, and *c* [Å]	*α*, *β*, and *γ* [°]	Cell volume [Å^3]
DPA	SCXRD[a]	orthorhombic	7.370, 11.664, 18.894		1624.1
	PXRD[b]	orthorhombic	11.689, 18.992, 7.376		1637.5
[Na(DPA)]·H_2O	PXRD	triclinic	10.066, 17.247, 8.859	96.18, 93.48, 76.68	1487.0
[K(DPA)]·0.5H_2O	SCXRD	monoclinic	10.986, 13.054, 12.184	94.26	1742.5
	PXRD	monoclinic	12.181, 13.024, 10.968	94.37	1735.0
[Rb(DPA)]·H_2O	SCXRD	monoclinic	11.021, 13.262, 12.243	94.19	1784.6
	PXRD	monoclinic	12.287, 13.245, 11.005	94.16	1786.3
[Cs(DPA)]	SCXRD	monoclinic	13.885, 10.625, 11.500	91.63	1695.9
	PXRD	monoclinic	13.911, 10.643, 11.541	91.56	1707.9

[a] SCXRD = Single-crystal X-ray diffraction. [b] PXRD = Powder X-ray diffraction.

whereas those of **2**–**4** were monoclinic, i.e., the same as that of single crystals of **2**–**4** reported above. The unit cell dimension and volume of the cell obtained from powder and single-crystal X-ray data also matched well.

Discussion

As mentioned above, selectivity was estimated through analysis of the precipitate obtained when a mixture of cations (bittern comprising mainly Na^+, K^+ and Mg^{2+} in one case and K^+, Rb^+ and Cs^+ in another case) was contacted with aqueous $Ca(DPA)_2$. When bittern is used, K^+ is found to be highly selective whereas Cs^+ is the most selective when the mixture comprises K^+, Rb^+ and Cs^+. To rationalize the observations of the second case, we sought to establish whether bulk precipitates are structurally similar to the single-crystal structures so that the latter may provide an understanding of selectivity. The similarity between experimental powder XRD data of bulk precipitates of **2**–**4** − that are formed almost instantaneously − and simulated diffractograms from the single-crystal data (Figure 7),[9] lead us to propose that the former are indeed structurally similar to the latter and, therefore, understanding of the crystal structures may provide vital clues on the selectivity trend. The unit cell dimensions obtained from powder X-ray data of **2**–**4** also matched well with those obtained from single-crystal X-ray data (Table 3) providing further support to this thesis. A similar comparison was not possible in the case of **1** in view of the inability to grow its single crystal.

As can be seen from the single-crystal structures of **2**–**4**, these structures are held in place by M···O and C–H···O interactions. Reduced exposure of the polar groups of the ligand to water by tying these up internally in the structure would lead to reduced solubility and, consequently, precipitation. The precipitation of $M^{n+}(DPA)_n$ can be depicted by Equation (1) (see also Scheme 1).

$$M^+_{(aq)} + [Ca(DPA)_2]_{aq} \rightarrow M(DPA)_n\downarrow + Ca^{2+}_{(aq)} \quad (1)$$

It can be seen from Equation (1) that the reaction will be favored with decrease in hydration enthalpy of $M_{(aq)}{}^+$. The values of hydration enthalpies follow the trend: M^{2+} (Mg, Ca) >> Na^+ (–97 kcal/mol) >K^+ (–77 kcal/mol) > Rb^+ (–70 kcal/mol) > Cs^+ (–63 kcal/mol). Thus for the mixture of K^+, Rb^+, and Cs^+, the selectivity would be highest for Cs^+ and least for K^+.[10] For the bittern system comprising Na^+, K^+, and Mg^{2+}, K^+ would be expected to have the highest selectivity on the basis of hydration enthalpy alone.

However, there are, other factors that also control selectivity besides hydration enthalpy. From packing diagrams of the K^+, Rb^+, and Cs^+ compounds **2**–**4**, space-filling models of the respective cavities comprising the metal ion and metal-bound oxygen atoms have been generated. The diagram for **4** is given in the figure in the table of contents of this issue and those of **2** and **3** are deposited as Supporting Information (Figures S4 and S5). The eight oxygen atoms around K^+/Rb^+ and ten oxygen atoms around Cs^+ make near-spherical cavities, the diameters of which can be determined from the respective distances between the *trans* oxygen atoms. The approximate diameters of the cavities (average of the distances between the *trans* oxygen atoms having O–M–O angle > 150°) are 5.720, 5.865, and 6.561 Å for K^+, Rb^+, and Cs^+, respectively. This increasing order of diameter of the cavities qualitatively follows the increasing order of the ionic sizes of these ions (2.66 Å, 2.94 Å, and 3.34 Å, for K^+, Rb^+, and Cs^+, respectively).[11] However, compared to the differences in the sizes of K^+ and Rb^+, the difference in the cavity diameters is less pronounced. Two opposite factors control cavity size: (i) short M···O distance and small size of the cation that can reduce the size of the cavity, and (ii) steric hindrance and electrostatic repulsion that prevent ligands from coming closer, and thereby increasing the cavity size. In the case of K^+, the latter may be the more dominant factor that prevents further shrinkage of the cavity diameter and weakens the M···O interactions which may, in addition to the hydration enthalpy difference, account for its lower selectivity in comparison to Rb^+, despite the similarities of the structures. Na^+, having smaller ionic size (1.94 Å), may be too small to fit in this cavity to make significant M···O interaction to form a stable assembly, if a similar structure were to apply in its case also. Alternative structures are, of course, possible, but comparative NMR study of **1** and NaCl suggests lack of metal-ligand interaction in solution, as ^{23}Na signal of both of them appeared at the same position, i.e., their environments are likely to be the same, namely Na^+ in hydrated state.

In the case of Cs^+, a large upfield shift (δ = 49.7 ppm) of the ^{133}Cs NMR signal of **4**, compared to CsCl, indicates strong metal-ligand interactions in solution. Ten oxygen atoms in the vicinity of the metal ion make strong Cs^+···O interactions, which decreases effective positive charge on the metal ion resulting in shielding of the Cs^+ ion. The additional NMR signals, which grow in with progress of the experiment, could be due to some new species formed in solution by dissociation of the supramolecular assembly. However, in all cases the observed peaks are shifted upfield indicating significant Cs^+···O interactions in solution state. Thus the selective formation may be assumed to originate in the solution phase and cascades to the solid precipitates. The larger cavity size in **4** allows for a higher coordination number (10) of Cs^+, which may lead to a greater degree of stabilization of the structure than with Rb^+ and K^+. Differences in ligand conformations may also have an effect on energetics and, consequently, selectivity. It is interesting to note that the DPA^- conformation in **4** has the closest match to that of DPA in crystalline state, the mean plane distortion being 61.35° compared to 50.5° for neutral DPA.[5] The deviations are much larger for **2** & **3**.

Alkaline earth metal ions, which are divalent in nature and have much higher hydration enthalpies ((Mg^{2+}, –459.1 mkcal/mol; Ca^{2+}, –376.9 kcal/mol; Sr^{2+}, –344.9 kcal/mol; Ba^{2+}, –311.9 kcal/mol),[10] are more difficult to complex with DPA^- which accounts for the high solubility of $Ca(DPA)_2$ and the lack of any $Mg(DPA)_2$ precipitation despite its high concentration in bittern. The relatively small ionic sizes of these cations may also be another factor that

thwarts complex formation and precipitation. This is borne out by our preliminary studies with the larger Sr^{2+} and Ba^{2+} (ionic diameters: 2.26 and 2.68 Å, respectively) ions,[11] wherein crystals of $[Sr(DPA)_2]\cdot 4H_2O$ and $[Ba(DPA)_2]\cdot 4H_2O$ could be obtained from the solution on slow evaporation of the solvent.[12]

Conclusions

We conclude from the present study that the selectivity of formation of $[M^{n+}(DPA^-)_n]$ can be divided into two broad categories: (i) cations such as K^+, Rb^+, and Cs^+ that favorably form precipitates almost instantaneously upon contact and (ii) those such as Na^+ and Ca^{2+} that do not form any precipitate. The former case pertains to compounds where the cation and DPA^- readily form complexes. The latter case, as exemplified by the ^{23}Na NMR studies with aqueous Na(DPA) wherein the environment of Na^+ is the same as that of Na^+ in aqueous NaCl, pertains to the situation wherein complex formation is unfavorable for a variety of reasons such as large hydration enthalpy and unfavorable ionic size. Sr^{2+} and Ba^{2+} represent an intermediate case where the complexes are moderately soluble and crystal formation does occur, albeit sluggishly, upon slow evaporation of the solution. Where alkali metal ions precipitate instantaneously with DPA^-, the observed selectivities are nicely explained on the basis of the structures of the complexes, which, in turn, are controlled by the relative sizes and hydration enthalpies of the cations. Kinetic factors could also contribute to some degree towards the selectivities.

Experimental Section

Materials: Dipicrylamine was purchased from National Chemical Co., India and used as received. AR grade KCl, RbCl, CsCl, CaO, and NaOH were obtained from S. D. Fine Chemicals. Double distilled water was used for the synthesis of compounds and Milli-Q (Millipore Corporation) water was used for ion chromatographic study.

Instrumentation: Elemental analyses (C,H,N) were performed with a model 2400 Perkin–Elmer elemental analyzer. The UV/Vis spectra were recorded with a model 8452A Hewlett–Packard diode array spectrophotometer. Cation concentration was measured with a Dionex 500 ion chromatograph. NMR spectra were recorded in D_2O with a model DPX 200 Bruker FT NMR instrument. X-ray powder diffraction data were collected using Philips X′ Pert MPD system with Cu-K_α irradiation. Single-crystal structures were determined using either Enraf–Nonius CAD-4 or Bruker SMART APEX (CCD) diffractometers.

Selectivity Studies with DPA^-: Selectivity studies were carried out by precipitating metal ions as DPA^- salts from bittern (the mother liquor obtained after recovery of common salt from brine, which contains a mixture of Na^+, K^+, Mg^{2+}, Ca^{2+}, SO_4^{2-}, and Cl^-) and also from a solution containing equimolar amount of KCl, RbCl and CsCl. In a typical experiment $[Ca(DPA)_2]$ was prepared first by adding solid CaO (0.067 g, 1.2 mmol) into an aqueous (10 mL) suspension of DPA (0.439 g, 1 mmol) followed by stirring of the reaction mixture for 5 min. 10 mL of this (filtered) aqueous $[Ca(DPA)_2]$ (1 mmol) was added with stirring into bittern (20 mL) or into an aqueous solution (50 mL) containing 2 mmol each of KCl, RbCl, and CsCl. The precipitate, which was instantaneously separated, was isolated by filtration and washed with diethyl ether and dried in vacuo. 10 mg of this material was calcined at 550 °C in a furnace and the residue was dissolved in nitric acid, which was evaporated and the residue was further dissolved in deionised water (20 mL) and filtered through 0.2 μm filter paper. The concentrations of the metal ions in the filtrate were determined by ion chromatography using Ion Pac CS12 (2 mm) analytical column and 20 mM methylsulphonic acid as eluent with a flow rate of 0.25 mL/min. Quantification was made using standard solutions containing Na^+, K^+, Mg^{2+}, and Ca^{2+} in one case and K^+, Rb^+, and Cs^+ in the other case.

Synthesis of Metal Salts of DPA^-

$[Na(DPA)]\cdot H_2O$ (1): To an aqueous (10 mL) suspension of DPA (0.439 g, 1 mmol) 2 mL of NaOH (0.04 g) was added dropwise and the reaction mixture was stirred at room temperature for 2 h, during which a dark brown solution was formed. After stripping off the water in a rotavap, the dry mass was dissolved once again in 5 mL volume of water and filtered to remove traces of insoluble material. The water was then evaporated and the compound was dried in vacuo, yield 94% (0.45 g). $C_{12}H_6N_7NaO_{13}$ (479.0): calcd. C 30.09, H 1.26, N 20.46; found C 30.31, H 1.03, N 20.02. UV/Vis (H_2O): λ_{max} (ε) = 426 nm (3.3×10^4).

$[K(DPA)]\cdot 0.5H_2O$ (2). Method I, from Bittern: 10 mL of aqueous $[Ca(DPA)_2]$ (1 mmol) was added into bittern (10 mL) and stirred for 5 min. The brown precipitate, which formed almost instantaneously, was isolated by filtration, washed with water and diethyl ether and recrystallised from a large volume of water. Yield: 0.41 g (85%). **Method II, from KCl:** Solid KCl (0.075 g, 1 mmol) was added into the above-mentioned dark brown solution (Ca^{2+} salt of DPA^-) and stirring was continued for 5 min, during which a brown precipitate was separated. The precipitate was isolated and purified following the procedure mentioned in method I, yield 86% (0.4 g). $C_{12}H_5KN_7O_{12.5}$ (486.1): calcd. C 29.65, H 1.04, N 20.16; found C 29.70, H 0.95, N 19.90. UV/Vis (H_2O): λ_{max} (ε) = 426 nm (3.5×10^4).

$[Rb(DPA)]\cdot H_2O$ (3): This compound was synthesized following the same procedure as that described for method II of complex **2**, replacing KCl with RbCl, yield 85% (0.46 g). $C_{12}H_6N_7O_{13}Rb$ (541.5): C 26.61, H 1.12, N 18.09; found C 26.28, H 1.02, N 17. 86. UV/Vis (H_2O): λ_{max} (ε) = 426 nm (3.5×10^4).

$[Cs(DPA)]$ (4): This compound was synthesized following the same procedure as that described for method II of complex **2**, replacing KCl with CsCl, yield 84% (0.47 g). $C_{12}H_4CsN_7O_{12}$ (570.9): C 25.24, H 0.71, N 17.16; found C 25.19, H 0.86, N 17.11. UV/Vis (H_2O): λ_{max} (ε) = 426 nm (3.4×10^4).

X-ray Crystallography: Cell parameters and diffraction intensities for complex **2** were measured at room temperature with the CAD-4 X-ray diffractometer using graphite-monochromatised Mo-$K\alpha$ radiation (0.7107 Å) in the range θ = 2–25°, for complexes **3** and **4** data were collected on the CCD diffractometer (Table 4). In the case of complex **2**, 25 reflections with θ in the range 9–12° were used for getting the accurate cell dimensions. Three standard reflections were monitored after every 100 reflections during the entire period of data collection, which showed no significant variation, indicating the stability of the crystal. The crystal orientation, refinement of the cell parameters and intensity measurements were carried out using the program CAD-4 PC.[13] Raw intensity data were corrected for Lorentz polarization effects but not for absorp-

tion. The Lorentz polarization corrections and data reduction were carried out using NRCVAX program.[14] The data for DPA and complexes **3** and **4** were corrected for Lorentz polarization and absorption effects. SHELXL-97[15] was used for structure solution and full-matrix least-squares refinement on F^2 for all these data. H atoms were included in the structure as riding model or obtained from the difference Fourier map.

Table 4. Summary of crystallographic data for **2**–**4**.

Compound	**2**	**3**	**4**
Empirical formula	$C_{12}H_4KN_7O_{12.5}$	$C_{12}H_4N_7O_{13}Rb$	$C_{12}H_4CsN_7O_{12}$
Molecular mass	485.32	539.69	571.13
Crystal system	monoclinic	monoclinic	monoclinic
Space group	$P2_1/n$	$P2_1/n$	$C2/c$
a [Å]	10.986 (4)	11.021(4)	13.885(5)
b [Å]	13.054(5)	13.262(5)	10.625(4)
c [Å]	12.184(3)	12.243(4)	11.500(4)
α [°]	90.0	90.0	90.0
β [°]	94.26(2)	94.190(5)	91.369(6)
γ [°]	90.0	90.0	90.0
Z	4	4	4
V [Å^3]	1742.5(10)	1784.6(11)	1695.9(11)
λ (Mo-K_α) [Å]	0.07107	0.7107	0.7107
$\rho_{calcd.}$ [g cm^{-3}]	1.850	2.869	2.276
μ [cm^{-1}]	8.930	28.69	22.76
T [K]	295(2)	295(2)	295(2)
R (F_o^2)[a]	0.0519	0.0342	0.0316
R_w (F_o^2)[b]	0.1302	0.0910	0.0788

[a] $R = \Sigma||F_o| - |F_c||/\Sigma|F_o|$, [b] $Rw = [Sw\ (F_o^2 - F_c^2)^2]/S\ [w(F_o^2)^2]^{1/2}$, $w = 1/\sigma(F_o)^2$:.

Powder X-ray Data Collection: Data were collected at room temperature in continuous scan mode in the 2θ range 5–60° with a step size of 0.02° 2θ and a count time of 4 s per step. Powder patterns were indexed using Visser-ITO[16] indexing program.

Simulation: Powder XRD pattern was simulated from single-crystal data by the method of Speak, using standard PLATON software.[9]

CCDC-264106 to -264108 (for **2**–**4**) contain the supplementary crystallographic data for this paper. These data can be obtained free of charge from The Cambridge Crystallographic Data Centre via www.ccdc.cam.ac.uk/data_request/cif.

Supporting Information Available: Ion chromatograms of a standard solution containing mixture of ions (Na^+, K^+, Mg^{2+}, Ca^{2+}), bittern and extracted (by DPA^-) material (Figure S1, see footnote on the first page of this article), PLUTO view of **3** showing metal–oxygen interactions (S2), molecular packing diagram of **3** showing the architecture, in which the metal ions are encapsulated (S3) and space filling models of the cavity consisting of metal ion and coordinated oxygen atoms for complexes **2** and **3** (Figures S4 and S5).

Acknowledgments

We are grateful to the Department of Science and Technology (DST), Government of India, for financial support. We thank Dr. M. M. Bhadbhade, NCL, Pune, for crystallographic data collection of complexes **3** and **4**. The assistance of Dr. P. Dastidar in generating some of the figures is gratefully acknowledged. We also thank the referees for their valuable suggestions.

[1] a) A. Winkel, D. I. H. Maas, *Angew. Chem.* **1936**, *49*, 827; b) J. Kielland, *Patent*, **1940**, No. Au 109552 19400110; **1941**, No. DE 715199 19411120; c) J. Kielland, W. Fleischer, *Patent*, **1940**, No. AU 112196 19401219; d) E. Berner, J. Kielland, *Patent*, **1942**, No. DE 726545 19420903; e) F. Massazza, B. Riva, *Ann. Chim. (Rome)* **1958**, *48*, 664; F. Massazza, B. Riva, *Ann. Chim. (Rome)* **1961**, *51*, 645; f) J. N. Kapoor, J. M. Sarkar, *Technology (Sindri, India)* **1966**, *3*, 177; g) S.-K. Chu, C.-T. Liaw, *Huaxue* **1969**, *4*, 106; h) J. Kielland, *Chem. Indust.* **1971**, 1309; i) M. Y. Bakr, A. A. Zatout, *Chemical Economy & Engineering Rev.* **1979**, *11*, 31.

[2] L. A. Bray, E. C. Martin, R. L. Moore, W. A. Richland, *U. S. At. Energy Commun.* **1962**, *HW-SA-2620*, p. 8.

[3] a) M. Kyrs, J. Pelcik, P. Polansky, *Czech. Collection Czechoslov. Chem. Communs.* **1960**, *25*, 2642; b) V. Kourim, J. Krtil, *Proc. U. N. Intern. Conf. Peaceful Uses At. Energy*, 2nd, Geneva, **1958**, *28*, 139; c) J. Rais, P. Selucky, *Patent*, **1973**, No. CZXXA9 CS 149403 19730715.

[4] a) M. L. Kundu, J. N. Kapoor, S. K. Ghosh, *Proc. Indian Acad. Sci., Chem. Sci.* **1982**, *91*, 65; b) K. Wozniak, H. He, J. Klinowski, W. Jones, E. Grech, *J. Phys. Chem.* **1994**, *98*, 13755.

[5] K. Wozniak, P. R. Mallinson, C. C. Wilson, E. Hovestreydt, E. Grech, *J. Phys. Chem. A* **2002**, *106*, 6897.

[6] a) M. L. Kundu, S. K. Ghosh, *Acta Crystallogr., Sect. B* **1980**, *36*, 941; b) V. P. Chalyi, F. G. Kramarenko, Yu. P. Krasan, L. L. Shevchenko, *Ukrainskii Khimicheskii Zhurnal* **1980**, *46*, 227; c) S. Furberg, P. Larssen, *Acta Chem. Scand.* **1952**, *6*, 965; d) V. P. Chalyi, G. N. Novitskaya, Yu. P. Krasan, L. L. Shevchenko, A. T. Pilipenko, *Zhurnal Strukturnoi Khimii* **1974**, *15*, 159.

[7] a) J. D. Owen, M. R. Truter, J. N. Wingfield, *Acta Crystallogr., Sect. C* **1984**, *40*, 1515; b) T. Sakamaki, Y. Inaka, Y. Nawata, *Acta Crystallogr. Sec. B* **1976**, *32*, 768; c) T. Sakamaki, Y. Inaka, Y. Nawata, *Chem. Lett.* **1972**, 1225; d) P. B. Hitchcock, M. F. Lappert, A. V. Protchenko, *J. Am. Chem. Soc.* **2001**, *123*, 189; e) K. Fukaya, T. Yamase, *Angew. Chem. Int. Ed.* **2003**, *42*, 654.

[8] a) P. R. A. Webber, G. Z. Chen, M. G. B. Drew, P. D. Beer, *Angew. Chem. Int. Ed.* **2001**, *40*, 2265; b) M. Cai, A. L. Marlow, J. C. Fettinger, D. Fabris, T. J. Haverlock, B. A. Moyer, J. T. Davis, *Angew. Chem. Int. Ed.* **2000**, *39*, 1283.

[9] A. L. Speak, *PLATON - A multipurpose crystallographic tool*, Ultrecht Univ., Ultrecht, The Netherland, *Acta Crystallogr., Sect. A* **1990**, *46*, C34.

[10] C. J. Pedersen, *J. Am. Chem. Soc.* **1967**, *89*, 7017.

[11] F. A. Cotton, W. Wilkinson, *Advanced Inorganic Chemistry, A comprehensive Text*, 3rd ed. **1979**, pp. 198, 645.

[12] Preliminary crystallographic data confirmed the compositions $[Sr(DPA)_2]\cdot 4H_2O$ and $[Ba(DPA)_2]\cdot 4H_2O$ with ten M···O interactions, however, well refined structures are yet to be obtained.

[13] *CAD4-PC Software*, Version 5, Enraf–Nonius, Delft, **1989**.

[14] E. I. Gabe, Y. Le Page, I. P. Charland, F. L. Lee, P. S. White, *J. Appl. Crystallogr.* **1989**, *22*, 384.

[15] G. M. Sheldrick, *SHELXL-97. Program for Crystal Structure Determination*, University of Göttingen, Germany, **1997**.

[16] J. W. Visser, *J. Appl. Crystallogr.* **1969**, *2*, 89.

Received: December 16, 2004

